DOI: 10.13009/EUCASS2019-1034

DOI:

Numerical Efficiency Analysis of Multi-pole Time-domain Impedance Boundary Conditions

Chao Chen⋆ *and Xiaodong Li*⋆†
⋆*School of Energy and Power Engineering, Beihang University*
Xueyuan Road 37, 100191, Beijing, P.R. China
chenc@buaa.edu.cn · lixd@buaa.edu.cn
†Corresponding author

Abstract

A modified multi-pole impedance model and corresponding time-domain broadband impedance boundary condition (TDIBC) is developed. It is validated by a two dimensional case in which the reflection of an acoustic line source by an infinite impedance surface with uniform mean-flow is solved numerically. The numerical efficiency and accuracy of the time-domain impedance boundary condition is then analyzed. It is found that the number and positions of the poles in the impedance model are the key factors that have an influence on the computational time. However, they barely affect the accuracy of the numerical results.

1. Introduction

Fan noise is one of the most important components of turbofan engine noise. Nacelle acoustic liner is one of the efficient noise suppression method to prevent the fan noise radiating to far field. The acoustic lining is a perforated sheet mounted on a honeycomb core with an impervious backing plate. For numerical investigation, it is extremely time-consuming to resolve all the resonators to evaluate the acoustic performance. In order to avoid modeling the realistic acoustic liner structure, impedance models and corresponding impedance boundary conditions have been developed. With an aeroacoustic propagation solver, the simulation and optimization of acoustic liner are feasible.
Among the diverse impedance models, the multi-pole model is a purely numerical model which is generic and broadband. It is generally a summation of adjustable first- and second-order systems and to be tuned to fit the resistance and reactance values. Several alternative mathematical forms are available from previous literatures.[1,4,11,14]
Based on previous experience of using the multi-pole model, it is found that the time-step and accuracy wound be affected by the positions and number of the poles. Therefore, the numerical efficiency and accuracy of the time-domain multi-pole impedance boundary condition is analyzed in this paper. An overview of multi-pole impedance models and the modified model proposed in this paper are given in Section 2. Numerical model and algorithms are described in Section 3. Then the numerical results and analysis is given. Conclusions are made in the last section.

2. Multi-pole impedance model

2.1 An overview of multi-pole impedance models

In this section, an overview of multi-pole impedance models in the frequency domain is given. Reymen et al.[14] proposed an impedance model in the form of a partial fraction expansion with resudues A_j and poles ζ_j.

$$Z(\omega) = \sum_{j=1}^{N} \frac{A_j}{\mathrm{i}\omega - \zeta_j} \tag{1}$$

In practice, Reymen et al.[14] focused on fitting the impedance data give by the three-parameter model.[16] Hence, only a pair of complex conjugate poles is used to represent the model as given by Eq. (2).

$$Z(\omega) = \frac{A_1}{\mathrm{i}\omega - \zeta} + \frac{A_2}{\mathrm{i}\omega - \zeta^*} = \frac{a_1(\mathrm{i}\omega) + a_0}{(\mathrm{i}\omega - \alpha)^2 + \beta^2} \tag{2}$$

DOI: 10.13009/EUCASS2019-1034

The two complex conjugated poles are $\alpha \pm \mathrm{i}\beta$.
Bin et al.[1] proposed a linear sum of second-order frequency response functions (FRFs) model to represent the impedance. In their paper, four FRFs were used to obtain a good approximation of impedance data from NASA Langley.[10]

$$Z(\omega) = \sum_{j=1}^{N} \frac{a_1^j(\mathrm{i}\omega) + a_0^j}{b_2^j(\mathrm{i}\omega)^2 + b_1^j(\mathrm{i}\omega) + b_0^j} \tag{3}$$

Li et al.[11] proposed an improved multi-pole broadband impedance model,

$$Z(\omega) = a_0 + \frac{a_1}{\mathrm{i}\omega} + a_2(\mathrm{i}\omega) + \sum_{j=1}^{N}\left(\frac{A_j}{\mathrm{i}\omega - \zeta_j} + \frac{A_j^*}{\mathrm{i}\omega - \zeta_j^*}\right) \tag{4}$$

where A_j and ζ_j are complex parameters, $*$ denotes the complex conjugate. This model is a combination of three-parameter model[16] and a multi-pole model.
Dragna et al.[4] proposed a model which consists three terms.

$$Z(\omega) = a_0 + \sum_{j=1}^{M} \frac{a_j}{\mathrm{i}\omega - \lambda_j} + \sum_{j=1}^{N}\left(\frac{A_j}{\mathrm{i}\omega - \zeta_j} + \frac{A_j^*}{\mathrm{i}\omega - \zeta_j^*}\right) \tag{5}$$

where a_0 is the limit value of $Z(\omega)$ as ω tends to infinity, λ_j are real poles and ζ_j, ζ_j^* are a pair of complex conjugate poles.

2.2 A modified multi-pole model

The impedance model proposed in this paper can be presented as,

$$Z(\omega) = a_0 + \mathrm{i}\omega a_1 + \sum_{j=1}^{M} \frac{b_j}{\mathrm{i}\omega - \lambda_j} + \sum_{j=1}^{N}\left(\frac{A_j}{\mathrm{i}\omega - \zeta_j} + \frac{A_j^*}{\mathrm{i}\omega - \zeta_j^*}\right) \tag{6}$$

where a_0, a_1, b_j and λ_j are real numbers, and $\lambda_j \geqslant 0$. A_j and ζ_j are complex numbers and $\Re(\zeta_j) \geqslant 0$.

3. Numerical model and algorithms

3.1 Numerical model

Reflection of an acoustic line source by an infinite impedance surface with uniform mean-flow[3] as shown in Fig. 1 is solved numerically. The mach number is Ma = 0.5. The annular frequency is $\omega = 31$ and the corresponding acoustic impedance is $Z = 0.75 - (39/3100)\mathrm{i}$. A uniform mesh is designed in which $\Delta x = \Delta y = 0.004$. For comparison, a simulation of sound reflection by an infinite hard wall is conducted as well.

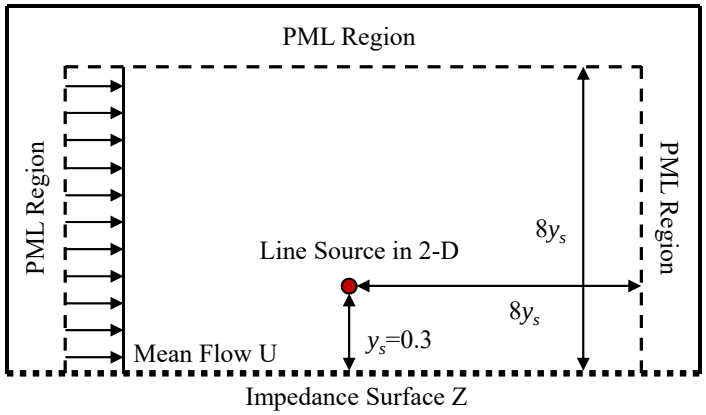

Figure 1: Sketch of the numerical model.

DOI: 10.13009/EUCASS2019-1034

Two models are used to achieve the target impedance at the given frequency. The first one is an ideal model,

$$Z(\omega) = R - \mathrm{i}\cot(\frac{\omega L}{c}) \tag{7}$$

where $R = 0.75$ and $L = 0.0502650434$. As show in Fig. 2, the resistance is constant for all frequencies and the reactance is a function of cotangent.

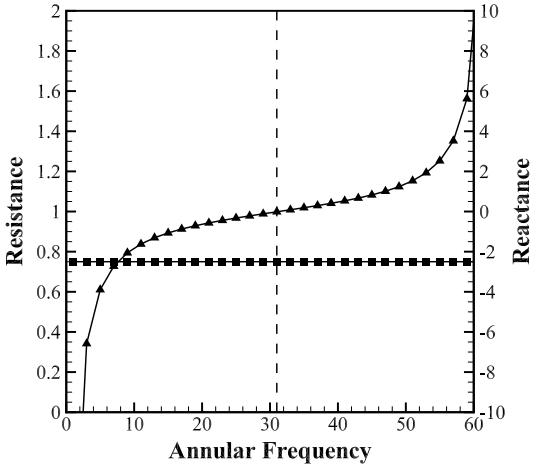

Figure 2: Acoustic impedance given by Eq. (7).

The second model deployed is this paper is Guess's model.[5] It is a semi-empirical model given by,

$$Z(\omega) = \frac{\sqrt{8\nu\omega}}{\sigma c}\left(1 + \frac{t}{d}\right) + \frac{\pi^2}{2\sigma}\left(\frac{d}{\lambda}\right)^2 + \frac{(1-\sigma^2)}{\sigma}\left[\frac{|\mathbf{u_0}|}{c} + kM\right] + \mathrm{i}\left[\frac{\omega(t+\delta)}{\sigma c} - \cot\left(\frac{\omega L}{c}\right)\right] \tag{8}$$

The unknown parameters in the formula are derived to meet the impedance at the target frequency and given in Table. 1. Figure 3 shows the impedance spectrum.

Table 1: Coefficients of Guess's impedance model

t **(mm)**	d **(mm)**	L **(mm)**	σ	δ **(mm)**	$\lvert\mathbf{u_0}\rvert$ **(m/s)**	k
1	1	347.521	17.3127%	0.33333	0.65257	0.25

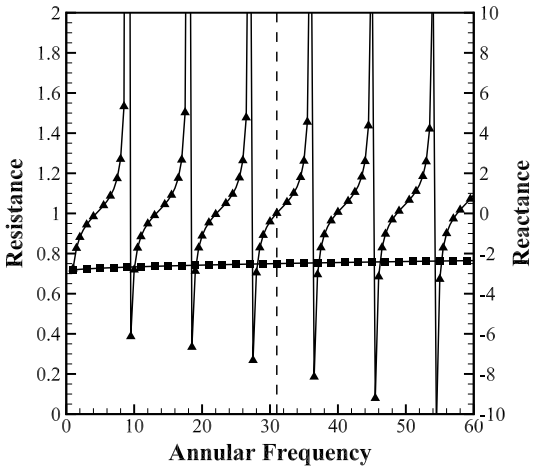

Figure 3: Acoustic impedance given by Eq. (8).

The vector fitting method[6] is used to determine the coefficients in the multi-pole models. The values of the coefficients and corresponding RMS errors are given in Appendix A2.

DOI: 10.13009/EUCASS2019-1034

3.2 Numerical algorithms

The two-dimensional linearized Euler equations (LEE) are adopted as the governing equations. The non-dimensional form is written as,

$$\frac{\partial \mathbf{U}}{\partial t} + \mathbf{A}\frac{\partial \mathbf{U}}{\partial x} + \mathbf{B}\frac{\partial \mathbf{U}}{\partial y} + \mathbf{D}\mathbf{U} = 0 \tag{9}$$

$$\mathbf{U} = \begin{pmatrix} \rho \\ u \\ v \\ p \end{pmatrix} \qquad \mathbf{A} = \begin{pmatrix} u_0 & \rho_0 & 0 & 0 \\ 0 & u_0 & 0 & \frac{1}{\rho_0} \\ 0 & 0 & u_0 & 0 \\ 0 & \gamma p_0 & 0 & u_0 \end{pmatrix}$$

$$\mathbf{B} = \begin{pmatrix} v_0 & 0 & \rho_0 & 0 \\ 0 & v_0 & 0 & 0 \\ 0 & 0 & v_0 & \frac{1}{\rho_0} \\ 0 & 0 & \gamma p_0 & v_0 \end{pmatrix} \qquad \mathbf{D} = \begin{pmatrix} \frac{\partial u_0}{\partial x} + \frac{\partial v_0}{\partial y} & \frac{\partial \rho_0}{\partial x} & \frac{\partial \rho_0}{\partial y} & 0 \\ \frac{1}{\rho_0}\left(u_0\frac{\partial u_0}{\partial x} + v_0\frac{\partial u_0}{\partial y}\right) & \frac{\partial u_0}{\partial x} & \frac{\partial u_0}{\partial y} & 0 \\ \frac{1}{\rho_0}\left(u_0\frac{\partial v_0}{\partial x} + v_0\frac{\partial v_0}{\partial y}\right) & \frac{\partial v_0}{\partial x} & \frac{\partial v_0}{\partial y} & 0 \\ 0 & \frac{\partial p_0}{\partial x} & \frac{\partial p_0}{\partial y} & \gamma\left(\frac{\partial u_0}{\partial x} + \frac{\partial v_0}{\partial y}\right) \end{pmatrix}$$

An in-house code based on advanced computational aeroacoustic (CAA) methods is deployed to solve these equations numerically. The spatial discretization utilizes the seven points 4th order dispersion-relation-preserving (DRP) scheme proposed by Tam & Webb.[17] And the optimized 2-N storage 5/6 Runge-Kutta scheme[8,15] is implemented for time integration. An artificial selective filter proposed by Bogey & Bailly[2] is adopted in the numerical simulation to eliminate the unresolved short-wave components. In this paper, the filter coefficient is 0.0005 for the whole computational domain. In addition, an absorption boundary condition based on the perfectly matched layer method (PML) developed by Hu et al.[7] has been implemented. The discretization of the singular 2-D line source satisfies the fourth order moment and smoothness conditions.[13]

The Myers or Ingard-Myers boundary condition[9,12] is used in this paper in which the acoustic normal displacement and acoustic pressure are assumed continuous across the liner surface. It is a linearized frequency-domain boundary condition.

$$\tilde{p} = Z\tilde{\mathbf{u}}\cdot\mathbf{n} - \frac{\bar{\mathbf{u}}}{\mathrm{i}\omega}\cdot\nabla\tilde{p} + \frac{\tilde{p}}{\mathrm{i}\omega}\mathbf{n}\cdot(\mathbf{n}\cdot\nabla\bar{\mathbf{u}}) \tag{10}$$

The time-domain impedance boundary condition is derived by applying the inverse Fourier transform to Eq.(10),

$$p(t) = \int_0^t z(t-\tau)\mathbf{u}(\tau)\cdot\mathbf{n}\mathrm{d}\tau - \int_0^t \bar{\mathbf{u}}\cdot\nabla p(\tau)\mathrm{d}\tau + \int_0^t \mathbf{n}\cdot(\mathbf{n}\cdot\nabla\bar{\mathbf{u}})p(\tau)\mathrm{d}\tau \tag{11}$$

where $z(t)$ is the inverse Fourier transform of $Z(\omega)$,

$$z(t) = \frac{1}{2\pi}\int_{-\infty}^{+\infty} Z(\omega)e^{\mathrm{i}\omega t}\mathrm{d}\omega \tag{12}$$

The inverse Fourier transform of $Z(\omega)$ in Eq. (6) is,

$$z(t) = a_0\delta(t) + a_1\frac{\partial\delta(t)}{\partial t} + \sum_{j=1}^{M} b_j\mathrm{e}^{\lambda_j t}H(t) + \sum_{j=1}^{N} 2\mathrm{e}^{\Re(\zeta_j)t}\left[\Re(A_j)\cos(\Im(\zeta_j)t) - \Im(A_j)\sin(\Im(\zeta_j)t)\right]H(t) \tag{13}$$

where $\delta(t)$ is the Dirac function and $H(t)$ stands for the Heaviside function. Substituting Eq. (13) into Eq. (**??**),

$$p(t) = a_0 v_n(t) + a_1\frac{\partial v_n(t)}{\partial t} + \sum_{j=1}^{M} b_j\phi_j(t) + \sum_{j=1}^{N} 2\left[\Re(A_j)\chi_j^I(t) - \Im(A_j)\chi_j^{II}(t)\right] - \bar{u_i}\psi_j(t) + n_i n_j\frac{\partial\bar{u_i}}{\partial x_j}\Psi(t) \tag{14}$$

DOI: 10.13009/EUCASS2019-1034

where $\phi_j(t)$, $\chi_j^1(t)$, $\chi_j^2(t)$ and $\psi(t)$ are accumulators which are convolution calculation.

$$\phi_j(t) = \int_0^t \mathrm{e}^{\lambda_j(t-\tau)} v_n(\tau)\mathrm{d}\tau$$
$$\chi_j^I(t) = \int_0^t \mathrm{e}^{\Re(\zeta_j)(t-\tau)} \cos[\Im(\zeta_j)(t-\tau)] v_n(t)\mathrm{d}\tau$$
$$\chi_j^{II}(t) = \int_0^t \mathrm{e}^{\Re(\zeta_j)(t-\tau)} \sin[\Im(\zeta_j)(t-\tau)] v_n(t)\mathrm{d}\tau$$
$$\psi_j(t) = \int_0^t \frac{\partial p(\tau)}{\partial x_j}\mathrm{d}\tau$$
$$\Psi(t) = \int_0^t p(\tau)\mathrm{d}\tau$$

The evaluation of the convolution integral in Eq (14) is extremely time consuming. Bin et al.[1] and Dragna et al.[4] developed an auxiliary differential equations (ADE) method, also referred as a generalized recursive method to avoid the computationally heavy problem in calculating the convolution integral numerically. The fundamental idea of the ADE method is calculating the accumulators by a differential system which could be easily derived by differentiating the above equations.

$$\frac{\partial \phi_j}{\partial t} - \lambda_j \phi_j - v_n = 0 \tag{15}$$
$$\frac{\partial \chi_j^I}{\partial t} - \Re(\zeta_j)\chi_j^I + \Im(\zeta_j)\chi_j^{II} - v_n = 0 \tag{16}$$
$$\frac{\partial \chi_j^{II}}{\partial t} - \Re(\zeta_j)\chi_j^{II} - \Im(\zeta_j)\chi_j^I = 0 \tag{17}$$
$$\frac{\partial \psi_j(t)}{\partial t} - \frac{\partial p}{\partial x_j} = 0 \tag{18}$$
$$\frac{\partial \Psi(t)}{\partial t} - p = 0 \tag{19}$$
$$\tag{20}$$

In the numerical model used in this paper, the mean flow is $\bar{\mathbf{u}} = [u_0 \ 0 \ 0]^T$ and the normal vector on the impedance boundary is $\mathbf{n} = [0 \ 1 \ 0]$. Thus, the Ingard-Myers boundary condition could simplified as,

$$\tilde{p} = Z\tilde{v_n} - \frac{u_0}{\mathrm{i}\omega}\frac{\partial \tilde{p}}{\partial x} \tag{21}$$

The corresponding time-domain impedance boundary condition is,

$$p(t) = a_0 v_n(t) + a_1 \frac{\partial v_n(t)}{\partial t} + \sum_{j=1}^{M} b_j \phi_j(t) + \sum_{j=1}^{N} 2\left[\Re(A_j)\chi_j^I(t) - \Im(A_j)\chi_j^{II}(t)\right] - u_0 \psi_x(t) \tag{22}$$

4. Numerical results and discussion

Firstly, the maximum stable $\mathrm{CFL}_{\max}$ is tested for both the hard wall and soft wall cases. It is found that the $\mathrm{CFL}_{\max}$ could reach around 0.85 for the case with hard wall and with the three impedance models. The time cost for each configurations is given in Tabel 2. The CPU is Intel(R) Xeon (R) E5-2650 2.00 GHz and the memory is 32 GB. Ten cores are used for each simulation. The comparison indicates that the computational time increases due to the calculating of auxiliary difference equations is insignificant. For 4 poles, the simulation time almost doesn't increase. Even for 16 poles, it only needs 3.2% more time to get the results.

The instantaneous pressure fields with hard surface and impedance surface are given in Fig. 4 respectively. The CFL is 0.8. Obviously, the reflection of acoustic wave by the surface depends on the impedance. And as a consequence, the far-field directivity will change correspondingly. Figure 5 provides the directivity comparison of numerical results and

DOI: 10.13009/EUCASS2019-1034

Table 2: Computational time for 6×10^4 steps.

Case	HW	#1 (4 poles)	#2 (6 poles)	#3 (16 poles)
Cost Time (min)	630.3	634.5	637.3	650.5
Increase (%)	-	0.67%	1%	3.2%

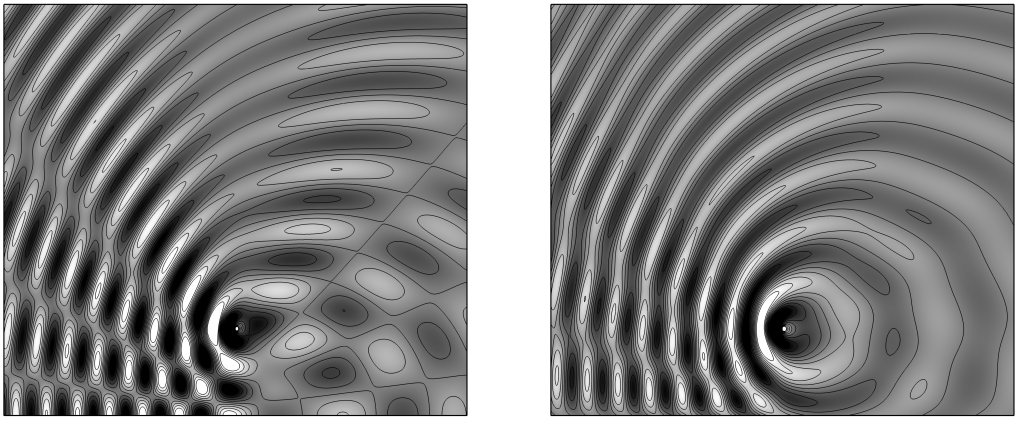

(a) Hard surface (b) Impedance surface

Figure 4: Instantaneous pressure field.

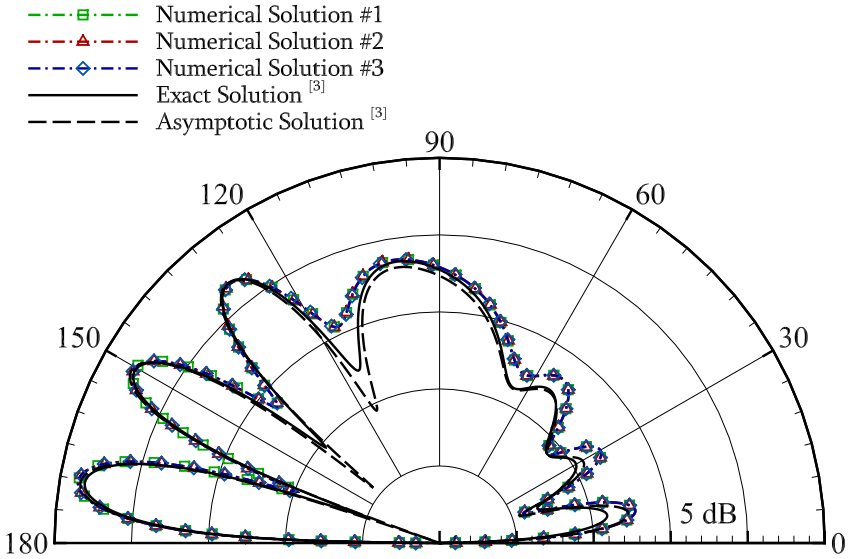

Figure 5: Directivity comparison.

analytical solutions.[3] The radius is $R = 2$ from the origin. The results agree with each other very well. All the seven lobes are correctly resolved.

Figure 6 depicts the directivity comparison of different CFL numbers. It is found that the numerical results with smaller CFL are general as the same as those with larger CFL number.

Previous investigation[11] shown that larger $\left|\Im(\zeta_j)\right|$ requires a smaller Δt to have a stable solution. A case with a pole having much larger $\left|\Im(\zeta_j)\right|$ is designed to check its influence on the Δt. The parameters are given in Table 3. In #4, $\left|\Im(\zeta_j)\right|$ is 100 times of it in #1 case. The target impedance at $\omega = 31$ remains. When the CFL equals 0.8, the boundary condition is not stable. As shown in Fig. 7, instability waves occur on the impedance boundary and grow rapidly. However, the solver becomes stable when the CFL decreases to around 0.3. Figure 8 shows the comparison of

DOI: 10.13009/EUCASS2019-1034

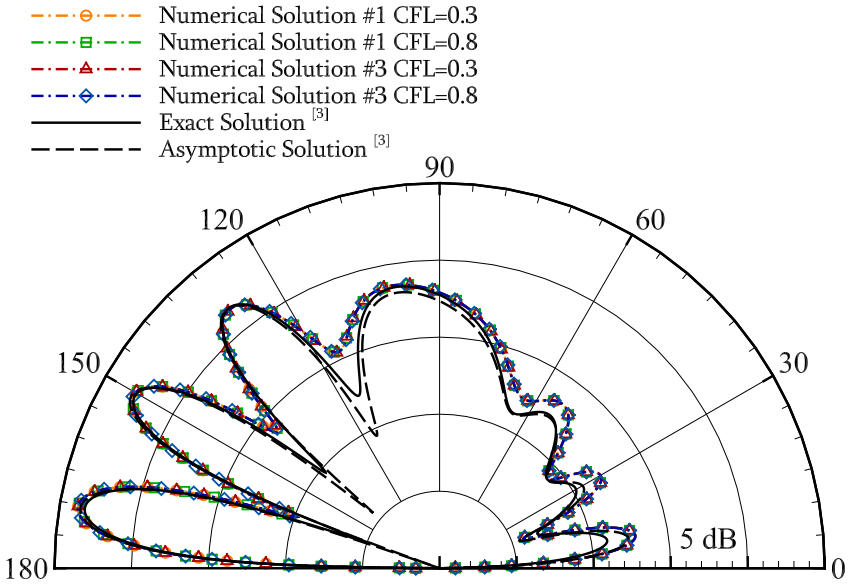

Figure 6: Directivity comparison.

the directivity of sound radiation. The results are nearly the same. Therefore, a pole with larger $\left|\Im(\zeta_j)\right|$ will require a much smaller Δt to keep the boundary stable, and it doesn't affect the numerical solutions when a stale CFL is used.

Table 3: Coefficients of the impedance model

No.	a_0	a_1	b_j	λ_j	A_j	ζ_j
#4	0.74873	0.02032	19.89724 0.08624	0.00013 -47.24916	20.16305+0.03386i	-0.00289+6251.56473i

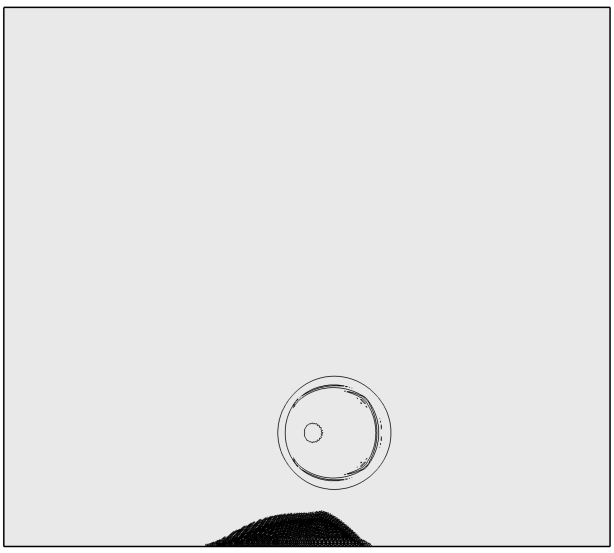

Figure 7: Instantaneous pressure field.

DOI: 10.13009/EUCASS2019-1034

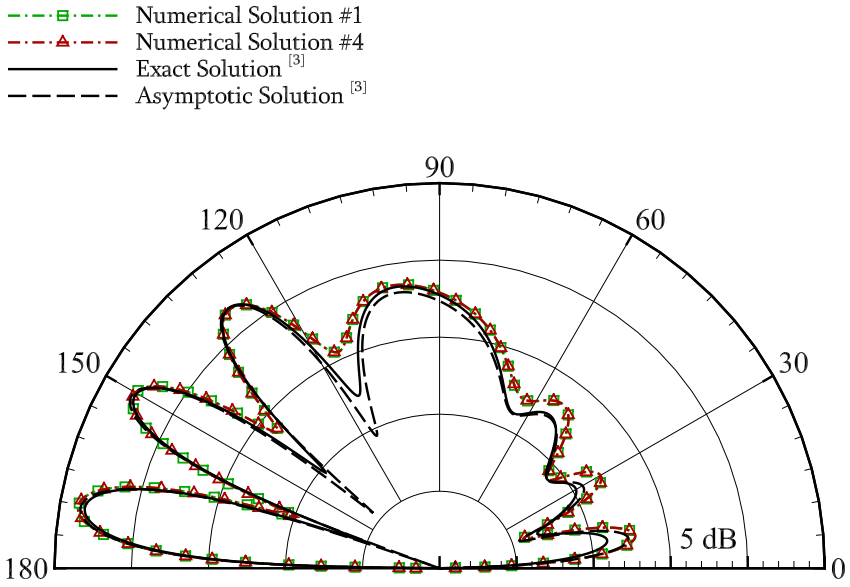

Figure 8: Directivity comparison.

5. Conclusion

A modified multi-pole impedance model is proposed. And the corresponding time-domain impedance boundary condition is derived. Numerical test shows that the maximum stable CFL could remain as the same as the hard wall case for poles have small $\left|\Im(\zeta_j)\right|$ in the model. The additional computational time due to the boundary condition increases little. Different impedance models and corresponding parameters make no difference in the results if the target acoustic impedance at a given frequency is achieved. However, if there is a pole or poles with large $\left|\Im(\zeta_j)\right|$ in the impedance model, the maximum stable CFL decreases. Mathematical analysis is needed to determine the relationship between $\mathrm{CFL}_{\max}$ and $\left|\Im(\zeta_j)\right|$ in the future.

Acknowledgments

This work is supported by grants from the National Science Foundation of China (91752204, 51476005), the IMAGE project and the 111 Project B07009 of China.

Appendix

A1. Definition

Assuming the fluctuating pressure and velocity fluctuations have time dependence, at $t \to \infty$, of the form,

$$p(\mathbf{x},t) = p(\mathbf{x})e^{\mathrm{i}(\omega t-\phi_{\mathbf{x}})}, \quad v(\mathbf{x},t) = v(\mathbf{x})e^{\mathrm{i}(\omega t-\phi_{\mathbf{x}})} \tag{23}$$

The Fourier transform and the inverse Fourier transform are defined as,

$$\tilde{f}(\omega) = \int_{-\infty}^{+\infty} f(t)e^{-\mathrm{i}\omega t}\mathrm{d}t, \quad f(t) = \frac{1}{2\pi}\int_{-\infty}^{+\infty} \tilde{f}(\omega)e^{\mathrm{i}\omega t}\mathrm{d}\omega \tag{24}$$

The convolution of two functions is defined as,

$$f * g(t) = \int_{-\infty}^{+\infty} f(t')g(t-t')\mathrm{d}t' \tag{25}$$

The acoustic impedance is defined as,

$$Z(\omega) = R(\omega) + \mathrm{i}X(\omega) = \frac{\tilde{p}(\omega)}{\tilde{\mathbf{u}}(\omega)\cdot\mathbf{n}} \tag{26}$$

DOI: 10.13009/EUCASS2019-1034

where ω is the angular frequency, R is referred as resistance and X is reactance, $\tilde{\mathbf{u}}(\omega) \cdot \mathbf{n}$ is the complex amplitude of the normal acoustic velocity pointing into the lined wall. The frequency depended acoustic impedance is normally either deduced from an experiment or predicted by a semi-empirical model. And the given impedance data is fitted by multi-pole impedance models, then the following numerical simulations could be conducted.

A2. Coefficients of the time-domain impedance model

Table 4: Coefficients of the impedance model for fitting Eq. (7)

No.	a_0	a_1	b_j	λ_j	A_j	ζ_j	RMS Error
#1	0.75501	0.00657	19.89731 -0.44701	-0.00007 -110.10225	20.17765 + 0.03071i	−0.00235 + 62.5156i	3.75×10^{-3}
#2	0.75376	0.002703	19.89454 -0.21241	0 -154.72834	19.89499 + 0.00006i 34.72416 + 0.20610i	−0.000002 + 62.50057i −0.17822 + 134.17739i	2.02×10^{-6}

Table 5: Coefficients of the impedance model for fitting Eq. (8)

No.	a_0	a_1	b_j	λ_j	A_j	ζ_j	RMS Error
#3	1.11441	0.01290	2.89215 -49.74967	-0.00604 -136.08284	2.88001 + 0.00201i 2.87882 + 0.00110i 2.87706 − 0.00014i 2.87529 + 0.00030i 2.87494 + 0.00053i 2.87915 + 0.00030i 5.53466 + 0.44668i	−0.00002 + 9.04004i −0.00003 + 18.08007i −0.00000 + 27.12006i −0.00005 + 36.15999i −0.00009 + 45.19984i −0.00002 + 54.23984i −0.22518 + 64.32188i	1.12×10^{-2}

References

[1] J. Bin, M. Yousuff Hussaini, and S. Lee. Broadband impedance boundary conditions for the simulation of sound propagation in the time domain. *The Journal of the Acoustical Society of America*, 125(2):664–675, 2009.

[2] C. Bogey and C. Bailly. A family of low dispersive and low dissipative explicit schemes for flow and noise computations. *Journal of Computational Physics*, 194(1):194–214, 2004.

[3] E. J. Brambley and G. Gabard. Reflection of an acoustic line source by an impedance surface with uniform flow. *Journal of Sound and Vibration*, 333(21):5548–5565, 2014.

[4] D. Dragna, P. Pineau, and P. Blanc-Benon. A generalized recursive convolution method for time-domain propagation in porous media. *The Journal of the Acoustical Society of America*, 138(2):1030–1042, 2015.

[5] A. W. Guess. Calculation of perforated plate liner parameters from specified acoustic resistance and reactance. *Journal of Sound and Vibration*, 40(1):119–137, 1975.

[6] B. Gustavsen and A. Semlyen. Rational approximation of frequency domain responses by vector fitting. *IEEE Transactions on Power Delivery*, 14(3):1052–1061, 1999.

[7] F. Q. Hu. A perfectly matched layer absorbing boundary condition for linearized euler equations with a non-uniform mean flow. *Journal of Computational Physics*, 208(2):469–492, 2005.

[8] F. Q. Hu, M. Y. Hussaini, and J. L. Manthey. Low-dissipation and low-dispersion runge-kutta schemes for computational acoustics. *Journal of Computational Physics*, 124(1):177–191, 1996.

[9] U. Ingard. Influence of fluid motion past a plane boundary on sound reflection, absorption, and transmission. *The Journal of the Acoustical Society of America*, 31(7):1035–1036, 1959.

DOI: 10.13009/EUCASS2019-1034

[10] M. G. Jones, W. R. Watson, and T. L. Parrott. Benchmark data for evaluation of aeroacoustic propagation codes with grazing flow. In *11th AIAA/CEAS Aeroacoustics Conference*, pages AIAA Paper 2005–2853, Monterey, USA, 2005. AIAA Inc.

[11] X. Y. Li, X. D. Li, and C. K. W. Tam. Improved multipole broadband time-domain impedance boundary condition. *AIAA Journal*, 50(4):980–984, 2012.

[12] M. K. Myers. On the acoustic boundary condition in the presence of flow. *Journal of Sound and Vibration*, 71(3):429–434, 1980.

[13] N. A. Petersson, O. Oreilly, B. Sjögreen, and S. A Bydlon. Discretizing singular point sources in hyperbolic wave propagation problems. *Journal of Computational Physics*, 321:532–555, 2016.

[14] Y. Reymen, M. Baelmans, and W. Desmet. Efficient implementation of tam and auriault's time-domain impedance boundary condition. *AIAA Journal*, 46(9):2368–2376, 2008.

[15] D. Stanescu and W. G. Habashi. 2n-storage low dissipation and dispersion runge-kutta schemes for computational acoustics. *Journal of Computational Physics*, 143(2):674–681, 1998.

[16] C. K. W. Tam and L. Auriault. Time-domain impedance boundary conditions for computational aeroacoustics. *AIAA Journal*, 34(5):917–923, 1996.

[17] C. K. W. Tam and J. C. Webb. Dispersion-relation-preserving finite difference schemes for computational acoustics. *Journal of Computational Physics*, 107(2):262–281, 1993.